VSP

Advanced Robotics 25 (2011) 1577–1601

ADVANCED ROBOTICS
brill.nl/ar

Full paper

Effect of Scaling on the Performance and Stability of Teleoperation Systems Interacting with Soft Environments

Hyoung Il Son [a,*], **Tapomayukh Bhattacharjee** [b] **and Hideki Hashimoto** [c]

[a] Department of Human Perception, Cognition and Action, Max Planck Institute for Biological Cybernetics, Tübingen, Germany

[b] Cognitive Robotics Center, KIST, Seoul 136-791, South Korea

[c] Institute of Industrial Science, The University of Tokyo, 4-6-1 Komaba, Meguro-ku, Tokyo 153-8505, Japan

Received 3 August 2010; accepted 7 September 2010

Abstract

There is generally a tradeoff between stability and performance in haptic control systems. Teleoperation systems with haptic feedback are no exception. Scaling in these systems used in applications such as tele-microsurgical systems has further effects on the stability and performance. This paper focuses on those applications interacting with soft tissues and analyzes the effects of the scaling in an effort to increase the performance of these systems while maintaining the stability. Position tracking and kinesthetic perception are especially important in the tele-surgical systems and, hence, are used as the performance criteria. Quantitatively defined stability robustness, which is based on Llewellyn's absolute stability criterion, is used as a metric for stability analysis. Various choices of scaling factors, and human and environment impedances are then investigated. The proposed kinesthetic perception concept is validated using psychophysical experiments. Widely used bilateral control architectures such as the two-channel position–position, two-channel force–position and four-channel controls are specifically analyzed and evaluated using simulations and experiments with phantom soft tissues. Results also show that the force–position control architecture shows the best position tracking performance irrespective of the scaling factors while the four-channel controller shows the best kinesthetic perception capability.

Keywords

Scaled teleoperation, scaling, stability, kinesthetic perception, psychophysics

* To whom correspondence should be addressed. E-mail: hyoungil.son@kaist.ac.kr

DOI:10.1163/016918611X579547

1. Introduction

Teleoperation has been used in many applications, including hazardous environments [1], space applications [2], underwater environments [3], production [4] and medicine [5]. Position and force scaling is often necessary between the master and the slave in many applications [6, 7]. A teleoperation system with scaled-up power is efficient for the manipulation and assembly of heavy materials and parts in production applications [8]. Position control accuracy can be also increased by scaling down the position in micro-assembly and microsurgery [8–10].

In tele-microsurgery, the position tracking ability of the slave robot is a fundamental performance index. In addition, microsurgical applications require tasks and skills like micro-positioning, making incisions, micro-dissections and suturing small vessels, which in turn require precise detection, and discrimination abilities for effective performance, and are also important for reducing injury and trauma [11–13]. Hence, enhancement of human perception, including detection and discrimination abilities, is very important for these applications. However, this aspect has been neglected in deriving many such performance indices that have been used in the literature to date based on different considerations. Therefore, in this paper, the detection and discrimination of dynamical changes in the environments are formulated as an index of kinesthetic perception [14], and also used as the second performance criteria.

For teleoperation systems interacting with soft environments, fidelity was proposed by Cavusoglu *et al.* as a more effective performance objective than that of transparency, based on the claim that information about the relative changes of environment impedance is more important for interactions with soft tissues than knowledge of the environment impedance alone [12]. However, fidelity, which is their performance objective, is different from the idea of the discrimination ability based on the concept of Weber's Law. In addition, their work does not help to increase the detection ability for microsurgical environments. Gersem *et al.* [13] only considered the enhancement of the sensitivity to environmental stiffness and tried to increase the relative changes in the stiffness for teleoperation systems. However, the experimental results are suboptimal and not sufficient to support the claim of the enhancement of stiffness perception. Reproducibility and operationality have been analyzed as possible metrics to measure the transparency by Iida and Ohniski [15] but their approach, which is based on transparency-related performance indices, is fundamentally different from our proposed performance indices required to quantify the detection ability, the discrimination ability, and the kinesthetic perception of an operator for soft environments in a teleoperation system. Therefore, by using these metrics defined in Ref. [15], it will be difficult to measure the operator's perception abilities, such as to determine how well the operator can detect and discriminate soft tissues. The difference between the transparency-based control method and the perception-based control method is presented in detail in Ref. [16]. Malysz and Sirouspour have also redefined transparency objectives to enhance the stiffness discrimination threshold by including nonlinear and linear filtered map-

ping between the master and the slave [17]. According to their approach, the product of the position scaling factor and the force scaling factor, which is expressed as $k_{\mathrm{p}}^{-1}k_{\mathrm{f}}$ in their paper, has to be designed as greater than 1 to increase the discrimination ability. However, this decreases the stability robustness [14]. Also, their work is only applicable when a force channel is used in bilateral controllers, but it is difficult to use slave-side force sensors in telesurgical or tele-microsurgical applications [12]. In addition, their approach did not guarantee enhancement of the detection ability.

The effects of position and force scaling on the kinesthetic perception, position tracking and stability of the scaled teleoperation are studied in this paper. Absolute stability [18] is used for the stability robustness analysis, which is a less conservative condition compared to passivity. Effects of the operator or surgeon and the environment impedances are also analyzed at the level of stability robustness. New quantitative indices are proposed to measure the effects of control parameters on the performance and stability robustness of the scaled teleoperation systems interacting with soft tissues. The developed methods are evaluated and compared in terms of the position tracking ability, kinesthetic perception and stability robustness using popular types of bilateral control architectures, including the two-channel position–position (PP), two-channel force–position (FP) and four-channel (4C) controls. This paper extends the original idea [19] to deal with the 4C control and also includes a discussion of additional experimental results. Experiments are then conducted with phantom soft tissues based on the PP, FP and 4C controls, and results verify the theoretical analysis of effects of scaling factors on performance and stability.

2. System Modeling, Performance and Stability

2.1. Scaled Teleoperation System

A two-port network model of a scaled teleoperation system is illustrated in Fig. 1. The human operator and the environment are modeled as second-order linear time-invariant impedance models, $Z_{\mathrm{h}} = m_{\mathrm{h}}s + b_{\mathrm{h}} + k_{\mathrm{h}}/s$ and $Z_{\mathrm{e}} = m_{\mathrm{e}}s + b_{\mathrm{e}} + k_{\mathrm{e}}/s$, respectively. m_i, b_i and k_i $(i = \mathrm{h}, \mathrm{e})$ represent the inertia, viscosity and stiffness of the human operator and the environment, respectively, and f_{h}^* denotes the intended force input of the human operator.

The two-port network model shown in Fig. 1 consists of the master, the slave, a bilateral controller, and the scaling and communication channels. Relations among these components can be expressed using a hybrid matrix [18, 20]. The hybrid matrix is defined as:

$$\begin{bmatrix} f_{\mathrm{m}} \\ -\dot{x}_{\mathrm{s}} \end{bmatrix} = H \begin{bmatrix} \dot{x}_{\mathrm{m}} \\ f_{\mathrm{s}} \end{bmatrix} = \begin{bmatrix} h_{11} & h_{12} \\ h_{21} & h_{22} \end{bmatrix} \begin{bmatrix} \dot{x}_{\mathrm{m}} \\ f_{\mathrm{s}} \end{bmatrix}, \tag{1}$$

where f_{m} and $\dot{x}_{\mathrm{m}}$ denote the force and the velocity at the master, while f_{s} and $\dot{x}_{\mathrm{s}}$ are the force and the velocity at the slave, respectively.

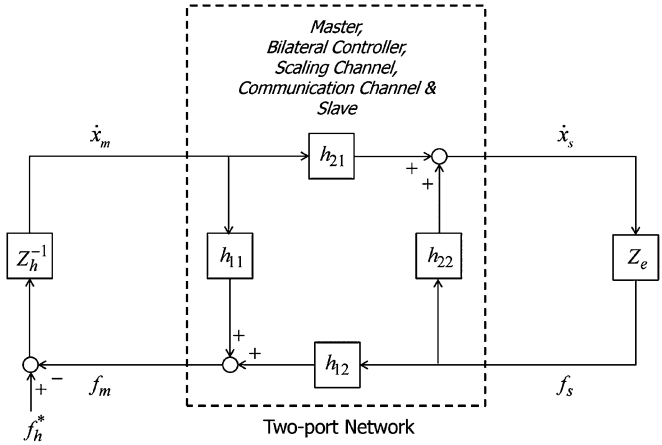

Figure 1. Two-port network model of a scaled teleoperation system.

Impedance transmitted to the human operator, Z_{to}, is derived using the hybrid matrix parameters as:

$$Z_{\text{to}} = \frac{h_{11} + (h_{11}h_{22} - h_{12}h_{21})Z_{\text{e}}}{1 + h_{22}Z_{\text{e}}}. \tag{2}$$

The position and force scaling factors are defined as S_{p} and S_{f}, respectively. Scaling laws for the position and the force are defined as $x_{\text{s}} = S_{\text{p}}x_{\text{m}}$ and $f_{\text{m}} = S_{\text{f}}f_{\text{s}}$, respectively. The hybrid matrix, therefore, becomes (3) in the case of perfect transparency [21]:

$$H_{\text{transparency}} = \begin{bmatrix} 0 & S_{\text{f}} \\ -S_{\text{p}} & 0 \end{bmatrix}, \tag{3}$$

and then Z_{to} simplifies to $S_{\text{p}}S_{\text{f}}Z_{\text{e}}$.

2.2. Performance: Position Tracking

Position tracking ability is evaluated in terms of the difference in the position between the master and the slave when there is no contact with the environment. Hence, position tracking is defined as:

$$\text{position tracking} = \left.\frac{x_{\text{m}} - x_{\text{s}}/S_{\text{p}}}{f_{\text{m}}}\right|_{f_{\text{e}}=0} = \frac{1}{h_{11}}\left(1 - \frac{h_{21}}{S_{\text{p}}}\right). \tag{4}$$

A performance index for the position tracking is defined quantitatively as:

$$PI_{\text{tracking}} = \left\| W_{\text{tracking}} \frac{1}{h_{11}}\left(1 - \frac{h_{21}}{S_{\text{p}}}\right) \right\|_2, \tag{5}$$

where W_{tracking} is a low-pass weighting function with a cut-off frequency $\omega_{\text{c,tracking}}$. Selection of $\omega_{\text{c,tracking}}$ depends on a particular application of the scaled teleoperation system. Since the normal tremor of a human hand occurs at 8–12 Hz [22], the $\omega_{\text{c,tracking}}$ is to be less than 8 Hz. A value of 2 Hz for $\omega_{\text{c,tracking}}$ can be some-

times considered reasonable in microsurgical applications since surgeons carry out surgery with very slow and careful movements [23, 24].

2.3. Performance: Kinesthetic Perception

Two types of thresholds are defined for perception based on the detection and discrimination of the kinesthetic stimuli in psychophysics [23, 25]. First, the absolute threshold (AL; absolute limen) is defined as the smallest amount of stimulus to produce a sensation in a detection task. This implies that the intensity of the stimuli has to be larger than the AL for it to be detected. The second is the difference threshold (DL; difference limen) which is defined as the smallest amount of stimulus change required to produce a change in sensation in a discrimination task. The linear relationship between DL and the stimulus intensity is known as Weber's law [25], and their ratio, which is defined as the DL over the initial intensity of the stimulus, is a constant more commonly known as the just noticeable difference (JND). Therefore, the discrimination ability, expressed in terms of the JND, varies with the reference stimulus intensity. Lower AL and JND values imply that detection and discrimination are relatively easier.

Impedance of the environment, Z_e, is the most important stimulus to perceive dynamic changes in the environment in telesurgery involving interaction with soft tissues [12, 14]. A kinesthetic perception region is defined in this paper to indicate a set of perceivable impedance levels of the environment based on AL, DL and JND. The kinesthetic perception region is illustrated in Fig. 2 [14, 19]. For example, it is impossible to detect Z_0^1 because it is smaller than AL. In addition, $Z_{\Delta t}^2$ cannot be discriminated from Z_0^2 because ΔZ^2 is smaller than DL. However, it is possible to perceive Z_0^3 and $Z_{\Delta t}^3$ because they satisfy the conditions of AL and DL. Therefore, the impedance transmitted to the human operator, Z_{to}, has to be located in the kinesthetic perception region to perceive the environment effectively. A larger area of kinesthetic perception region means better perception of the environment.

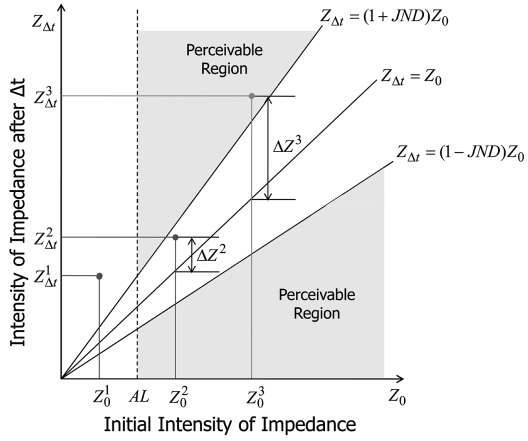

Figure 2. Kinesthetic perception region.

To compare the kinesthetic perception region quantitatively, two types of performance metrics are defined. First, the metric related to AL is defined in:

$$M_{\text{detection}} = \left\| W_{\text{perception}} \frac{Z_{\text{to}}}{Z_{\text{e}}} \right\|_2, \quad \text{where } \frac{Z_{\text{to}}}{Z_{\text{e}}} = \frac{h_{11}h_{22} - h_{12}h_{21} + h_{11}Z_{\text{e}}^{-1}}{1 + h_{22}Z_{\text{e}}}, \quad (6)$$

where $W_{\text{perception}}$ is a low-pass weighing function. The cut-off frequency $\omega_{\text{c,perception}}$ of $W_{\text{perception}}$ also depends on a particular application of the teleoperation system. Equation (6) represents the performance index for a detectable region, i.e., the detection ability.

The second metric related to JND, defined in (7), indicates the region in which stimuli can be discriminated, i.e., the discrimination ability:

$$M_{\text{discrimination}} = \left\| W_{\text{perception}} \frac{\Delta Z_{\text{to}}/Z_{\text{to}}}{\Delta Z_{\text{e}}/Z_{\text{e}}} \right\|_2,$$
$$\text{where } \frac{\Delta Z_{\text{to}}/Z_{\text{to}}}{\Delta Z_{\text{e}}/Z_{\text{e}}} = \frac{-h_{12}h_{21} + Z_{\text{e}}}{(1 + h_{22}Z_{\text{e}})[h_{11} + (h_{11}h_{22} - h_{12}h_{21})Z_{\text{e}}]}. \quad (7)$$

Finally, a quantitative performance index for the kinesthetic perception is defined in (8) using (6) and (7). The shaded area in Fig. 3 represents the index given in (8) [14, 19]:

$$PI_{\text{perception}} = (1 - \alpha) \cdot (1 - \beta),$$
$$\text{where } \alpha = \frac{1}{1 + M_{\text{detection}}} \text{ and } \beta = \frac{1}{1 + M_{\text{discrimination}}}. \quad (8)$$

The performance index of kinesthetic perception reaches unity in the case of ideal kinesthetic perception, which implies that the human operator can detect any magnitude of impedance and discriminate any changes in the impedance.

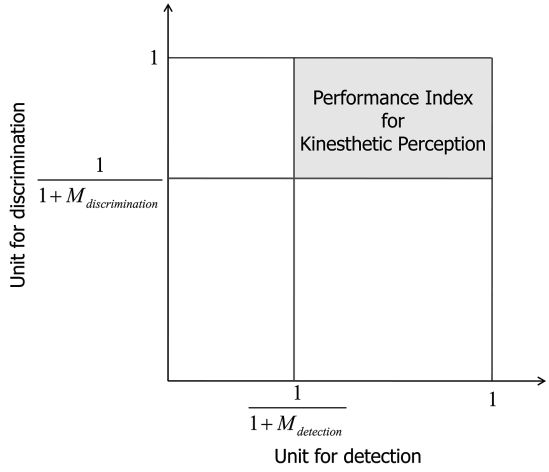

Figure 3. Performance index for kinesthetic perception.

2.4. Stability

Passivity analysis is a common approach to analyze the stability of a system. It guarantees the system stability coupled with the passive human operator and the environment. The net energy is calculated, which is the difference between the input energy and the output energy, and the system is passive if this difference is positive.

The operator dynamics, though passive, is generally adaptive and changing while the environment impedance is either unknown or inadequately modeled. Stability analysis based on the two-port network model of the scaled teleoperation system alone rather than the whole system including the operator and the environment is therefore more appropriate. When the two-port network of a teleoperation system remains stable under all possible uncoupled passive terminations, the teleoperation system is said to be absolutely stable. Absolute stability is used in this paper to analyze and evaluate the stability robustness of the scaled teleoperation system. Absolute stability is a less conservative condition when compared to passivity. Llewellyn's criterion for absolute stability is expressed in terms of immittance matrix parameters as follows [18, 26]:

- h_{11} and h_{22} have no poles in the right half plane.
- Any poles of h_{11} and h_{22} on the imaginary axis are simple with real and positive residues.
- For all the real values of ω, we have:

$$\begin{aligned} &\Re(h_{11}) \geqslant 0 \\ &\Re(h_{22}) \geqslant 0 \\ &2\Re(h_{11})\Re(h_{22}) - \Re(h_{12}h_{21}) - |h_{12}h_{21}| \geqslant 0. \end{aligned} \tag{9}$$

The last condition in (9) can be expressed as:

$$\eta = -\cos(\angle h_{12}h_{21}) + 2\frac{\Re(h_{11})\Re(h_{22})}{|h_{12}h_{21}|} \geqslant 1. \tag{10}$$

Stability robustness is analyzed and evaluated by defining η as the stability index [27]. However, it is difficult to compare the different levels of stability robustness quantitatively because this parameter varies over frequency. Therefore, a new metric is defined in this paper for quantitative analysis as illustrated in Fig. 4. First, the stability bandwidth is defined in (11), which refers to the maximum frequency that will maintain the system as stable. The stability robustness is, then, defined in (12) using the stability bandwidth:

$$\omega_{\text{bandwidth}}^{\text{stability}} = \max\{\omega_k \mid \forall\omega \leqslant \omega_k, \eta(\omega) \geqslant 1\} \tag{11}$$

$$\text{stability robustness} = \int_0^{\omega_{\text{bandwidth}}^{\text{stability}}} [\eta(\omega) - 1]\,\mathrm{d}\omega. \tag{12}$$

The stability index, defined in (10), does not include the human operator and environment impedance terms. However, a less conservative stability condition can

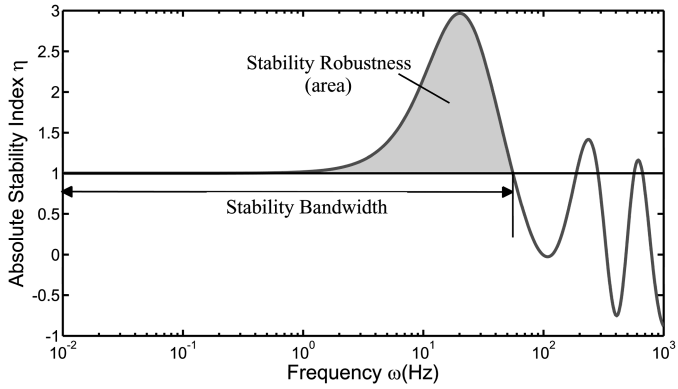

Figure 4. Performance index for stability robustness.

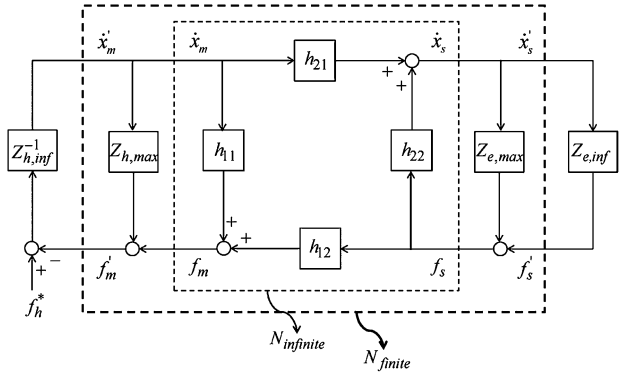

Figure 5. Extended two-port network model of a teleoperation system.

be derived by assuming the human operator and the environment are passive [27–29].

Therefore, the extended two-port network model of the scaled teleoperation system, shown in Fig. 5, can be used to extend the stability index of (10) to include the human operator and the environment impedances. First, the value representing the human operator impedance is divided into the actual maximum impedance of the human operator, $Z_{\mathrm{h,max}}$, which has a finite magnitude, and the nominal impedance of the human operator, $Z_{\mathrm{h,inf}}$, with infinite magnitude. The environment impedance can also be divided into the actual maximum impedance $Z_{\mathrm{e,max}}$ and the nominal impedance $Z_{\mathrm{e,inf}}$ [27].

Considering the extended two-port network N_{finite} shown in Fig. 5, the following new hybrid matrix form can be derived:

$$\begin{bmatrix} f_{\mathrm{m}} \\ -\dot{x}'_{\mathrm{s}} \end{bmatrix} = \begin{bmatrix} h'_{11} & h'_{12} \\ h'_{21} & h'_{22} \end{bmatrix} \begin{bmatrix} \dot{x}'_{\mathrm{m}} \\ f_{\mathrm{s}} \end{bmatrix}. \tag{13}$$

Here, (1) represents the hybrid matrix form of the two-port network N_{infinite}. Given $\dot{x}_{\text{m}} = \dot{x}'_{\text{m}} - f_{\text{m}}/Z_{\text{h,max}}$ and $\dot{x}'_{\text{s}} = \dot{x}_{\text{s}} - f_{\text{s}}/Z_{\text{e,max}}$, (1) takes the following form:

$$\begin{bmatrix} f_{\text{m}} \\ -\dot{x}'_{\text{s}} - \frac{f_{\text{s}}}{Z_{\text{e,max}}} \end{bmatrix} = \begin{bmatrix} h_{11} & h_{12} \\ h_{21} & h_{22} \end{bmatrix} \begin{bmatrix} \dot{x}'_{\text{m}} - \frac{f_{\text{m}}}{Z_{\text{h,max}}} \\ f_{\text{s}} \end{bmatrix}. \tag{14}$$

The new hybrid matrix form becomes:

$$\begin{bmatrix} f_{\text{m}} \\ -\dot{x}'_{\text{s}} \end{bmatrix} = \begin{bmatrix} \frac{h_{11}Z_{\text{h,max}}}{Z_{\text{h,max}}+h_{11}} & \frac{h_{12}Z_{\text{h,max}}}{Z_{\text{h,max}}+h_{11}} \\ \frac{h_{21}Z_{\text{h,max}}}{Z_{\text{h,max}}+h_{11}} & h_{22} - \frac{h_{12}h_{21}}{Z_{\text{h,max}}+h_{11}} + \frac{1}{Z_{\text{e,max}}} \end{bmatrix} \begin{bmatrix} \dot{x}'_{\text{m}} \\ f_{\text{s}} \end{bmatrix}. \tag{15}$$

Assuming that the performance of the scaled teleoperation system becomes transparent, implying that h_{11} is much smaller than $Z_{\text{h,max}}$, the new hybrid matrix form is finally expressed by:

$$\begin{bmatrix} f_{\text{m}} \\ -\dot{x}'_{\text{s}} \end{bmatrix} = \begin{bmatrix} h_{11} & h_{12} \\ h_{21} & h_{22} - \frac{h_{12}h_{21}}{Z_{\text{h,max}}} + \frac{1}{Z_{\text{e,max}}} \end{bmatrix} \begin{bmatrix} \dot{x}'_{\text{m}} \\ f_{\text{s}} \end{bmatrix}. \tag{16}$$

A new stability index η_{extended} can be derived from (16), using the stability index defined in (10), as:

$$\begin{aligned} \eta_{\text{extended}} = &-\cos(\angle h_{12}h_{21}) + 2\frac{\Re(h_{11})}{|h_{12}h_{21}|}\left\{\Re(h_{22}) + \Re\left(\frac{1}{Z_{\text{e,max}}}\right)\right\} \\ &+ 2\frac{\Re(h_{11})}{|Z_{\text{h,max}}|}\cos\left(\angle\frac{-h_{12}h_{21}}{Z_{\text{h,max}}}\right). \end{aligned} \tag{17}$$

Consequently, the effects of the human operator and the environment impedances on the robustness of the stability can be analyzed and evaluated using the extended stability index (17).

3. Effect of Scaling Factors

Generalized 4C control architecture for a scaled teleoperation system is shown in Fig. 6. The master and the slave are modeled as the second-order linear time-invariant (LTI) impedance models Z_{m} and Z_{s}, respectively; C_{m} and C_{s} represent the position controllers of the master and the slave, respectively. In addition, C_1 and C_3 are the position and force controllers from the master to the slave, respectively, and C_2 and C_4 are the position and force controller from the slave to the master, respectively. In the scaling channel, S_{p} and S_{f} represent the position and force scaling factors, respectively. Finally, the time delay T in the communication channel is defined as e^{-sT}.

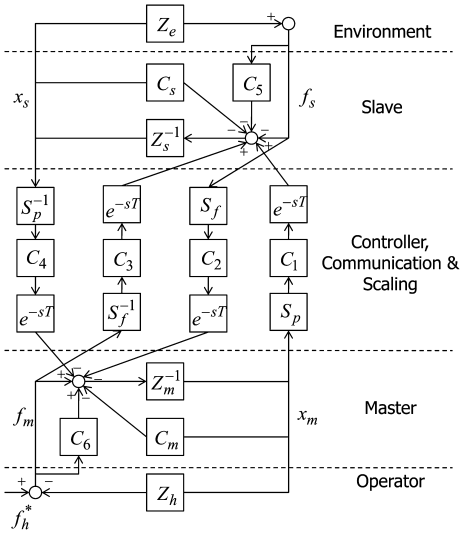

Figure 6. Generalized 4C control architecture with scaling and communication channel.

3.1. PP Control Architecture

PP control architecture is an architecture in which only the position information is transmitted between the master and the slave (i.e., $C_2 = C_3 = 0$). The hybrid matrix for PP control architecture is derived from Fig. 6:

$$H = \begin{bmatrix} \frac{Z_{cm}Z_{cs}+C_1C_4e^{-2sT}}{(1+C_6)Z_{cs}} & \frac{-S_p^{-1}C_4(1+C_5)e^{-sT}}{(1+C_6)Z_{cs}} \\ \frac{-S_pC_1e^{-sT}}{Z_{cs}} & \frac{1+C_5}{Z_{cs}} \end{bmatrix}. \tag{18}$$

The transmitted impedance to the operator Z_{to} is formulated using (2) and (13) as:

$$Z_{to} = \frac{Z_{cm}Z_{cs} + C_1C_4e^{-2sT} + (1+C_5)Z_{cm}Z_e}{(1+C_6)[Z_{cs} + (1+C_5)Z_e]}. \tag{19}$$

The first analysis of the PP control architecture involves position tracking. The derived equation for position tracking $(1 - h_{21}/S_p)/h_{11}$ is:

$$\frac{1}{h_{11}}\left(1 - \frac{h_{21}}{S_p}\right) = \frac{(1+C_6)(Z_{cs} + C_1e^{-sT})}{Z_{cm}Z_{cs} + C_1C_4e^{-2sT}}. \tag{20}$$

As shown in the numerator of (20), the accuracy of position tracking is not affected by the position scaling factor S_p. Additionally, decreasing the local force gain of the slave, C_6, also increases the accuracy of the position tracking.

In the case of kinesthetic perception, because Z_{to} does not contain any scaling factors as written in (19), $M_{detection}$ is not affected by the scaling factors. In addition, $h_{12}h_{21}$, as derived in (21), contains no scaling factors:

$$h_{12}h_{21} = \frac{C_1C_4(1+C_5)e^{-2sT}}{(1+C_6)Z_{cs}^2}. \tag{21}$$

As a result, there are no effects of the scaling factors on the kinesthetic perception of the PP control architecture because h_{11} and h_{22} do not contain scaling factors. In the same manner, scaling factors do not affect the stability robustness of the PP controller, as shown in (10).

In the case of the extended stability index η_{extended}, a lower magnitude of $Z_{\text{e,max}}$ makes the stability more robust. Essentially, lower $Z_{\text{h,max}}$ value also increases stability robustness. However the stability bandwidth is decreased when $Z_{\text{h,max}}$ is increased because $\cos(\angle -h_{12}h_{21})$ has a negative value at high frequencies.

3.2. FP Control Architecture

FP control architecture is an architecture where only the position information from the master to the slave and the force information from the slave to the master are available (i.e., $C_3 = C_4 = 0$). Equation (22) expresses the hybrid matrix of the FP control architecture:

$$H = \begin{bmatrix} \frac{Z_{\text{cm}}}{1+C_6} & \frac{S_{\text{f}}C_2\text{e}^{-sT}}{1+C_6} \\ \frac{-S_{\text{p}}C_1\text{e}^{-sT}}{Z_{\text{cs}}} & \frac{1+C_5}{Z_{\text{cs}}} \end{bmatrix}. \tag{22}$$

By substituting (22) into (2), Z_{to} is derived as:

$$Z_{\text{to}} = \frac{Z_{\text{cm}}Z_{\text{cs}} + [(1+C_5)Z_{\text{cm}} + S_{\text{p}}S_{\text{f}}C_1C_2\text{e}^{-2sT}]Z_{\text{e}}}{(1+C_6)[Z_{\text{cs}} + (1+C_5)]Z_{\text{e}}}. \tag{23}$$

Position tracking is formulated using (24). The position scaling factor S_{p} does not affect the position tracking accuracy of the FP controller similar to the PP control architecture. However, the FP control architecture has better position tracking compared to the PP control architecture as the denominator of $(1 - h_{21}/S_{\text{p}})/h_{11}$ for the FP controller is larger than that of the PP controller when $Z_{\text{cm}}Z_{\text{cs}} \gg Z_{\text{cm}}Z_{\text{cs}} + C_1C_4$:

$$\frac{1}{h_{11}}\left(1 - \frac{h_{21}}{S_{\text{p}}}\right) = \frac{(1+C_6)(Z_{\text{cs}} + C_1\text{e}^{-sT})}{Z_{\text{cm}}Z_{\text{cs}}}. \tag{24}$$

The first metric of the kinesthetic perception, $M_{\text{detection}}$, is increased with the increase of the product of scaling factors, $S_{\text{p}}S_{\text{f}} > 1$. This can be seen from (23). Additionally, given that $h_{12}h_{21}$ is formulated by (25), $M_{\text{discrimination}}$ is also increased as $S_{\text{p}}S_{\text{f}}$ increases. As a result, the kinesthetic perception region under the FP control architecture is increased with the increase of $S_{\text{p}}S_{\text{f}}$:

$$h_{12}h_{21} = \frac{-S_{\text{p}}S_{\text{f}}C_1C_2\text{e}^{-2sT}}{(1+C_6)Z_{\text{cs}}}. \tag{25}$$

However, the stability robustness will be decreased because $|h_{12}h_{21}|$ increases with an increase in the value of $S_{\text{p}}S_{\text{f}}$. Therefore, tradeoffs exist between stability and performance.

The extended stability robustness η_{extended} is also increased with the decrease of $Z_{\text{e,max}}$ and $Z_{\text{h,max}}$ for the same rationale of the PP control architecture.

3.3. 4C Control Architecture

The hybrid matrix is derived in (26) for 4C control architecture that uses all of the information pertaining to the position and the force between the master and the slave:

$$
\begin{aligned}
h_{11} &= \frac{Z_{\mathrm{cm}}Z_{\mathrm{cs}} + C_1C_4\mathrm{e}^{-2sT}}{(1+C_6)Z_{\mathrm{cs}} - S_{\mathrm{p}}^{-1}S_{\mathrm{f}}^{-1}C_3C_4\mathrm{e}^{-2sT}} \\
h_{12} &= \frac{S_{\mathrm{f}}C_2Z_{\mathrm{cs}}\mathrm{e}^{-sT} - S_{\mathrm{p}}^{-1}C_4(1+C_5)\mathrm{e}^{-sT}}{(1+C_6)Z_{\mathrm{cs}} - S_{\mathrm{p}}^{-1}S_{\mathrm{f}}^{-1}C_3C_4\mathrm{e}^{-2sT}} \\
h_{21} &= \frac{-S_{\mathrm{f}}^{-1}C_3Z_{\mathrm{cm}}\mathrm{e}^{-sT} - S_{\mathrm{p}}C_1(1+C_6)\mathrm{e}^{-sT}}{(1+C_6)Z_{\mathrm{cs}} - S_{\mathrm{p}}^{-1}S_{\mathrm{f}}^{-1}C_3C_4\mathrm{e}^{-2sT}} \\
h_{22} &= \frac{(1+C_5)(1+C_6) - C_2C_3\mathrm{e}^{-2sT}}{(1+C_6)Z_{\mathrm{cs}} - S_{\mathrm{p}}^{-1}S_{\mathrm{f}}^{-1}C_3C_4\mathrm{e}^{-2sT}}.
\end{aligned}
\tag{26}
$$

First, the effect of the scaling factor on position tracking is analyzed. The numerator of $(1 - h_{21}/S_{\mathrm{p}})/h_{11}$ has a $S_{\mathrm{f}}C_2\mathrm{e}^{-sT}$ term. Therefore, the accuracy of position tracking is increased with the increase of the force scaling factor. However, the position tracking accuracy of the 4C controller is inferior to that of the PP and FP controller as there are additional terms that are absent in the PP and FP controller, but present in the 4C controller in the numerator of $(1 - h_{21}/S_{\mathrm{p}})/h_{11}$.

For kinesthetic perception, the first metric $M_{\mathrm{detection}}$ increases with the increase in $S_{\mathrm{p}}S_{\mathrm{f}}$, as the numerator of $Z_{\mathrm{to}}/Z_{\mathrm{e}}$ contains $S_{\mathrm{p}}S_{\mathrm{f}}C_1C_2\mathrm{e}^{-2sT}$, which also applies to the case of the FP control architecture. In addition, $M_{\mathrm{detection}}$ increases more than $M_{\mathrm{detection}}$ in the FP control architecture with the increase in $S_{\mathrm{p}}S_{\mathrm{f}}$, as the denominator of $M_{\mathrm{detection}}$ contains $-S_{\mathrm{p}}^{-1}S_{\mathrm{f}}^{-1}C_3C_4\mathrm{e}^{-2sT}$. $M_{\mathrm{discrimination}}$ also increases more in the case of the FP controller for the same reason as that of $M_{\mathrm{detection}}$. Therefore, the kinesthetic perception region of the 4C control architecture is enlarged more than that of the FP control architecture with an increases in $S_{\mathrm{p}}S_{\mathrm{f}}$. Finally, the stability robustness also decreases with an increase in $S_{\mathrm{p}}S_{\mathrm{f}}$, as in the case of the FP control architecture. Also, the stability margin is decreased with increasing time delay and increased stiffness of the environment for 4C control architecture as well as PP and FP control architecture; however, the analyses of those aspects are not the main focus of our work as it is already widely known and hence accepted in contemporary work.

4. Psychophysical Experiment

Psychophysical experiments have been conducted to explain the physical meaning of the proposed kinesthetic perception, and to show its effectiveness in comparing the detection and discrimination abilities of human operators for different force feedback schemes.

4.1. Participants

For both these experiments, six subjects of different backgrounds and gender, falling in the age group of 21–29 years, are chosen to maintain the generality of the experiments. Two of them are from a technical background with no knowledge of haptics or psychophysics, while the others are familiar with haptics. Five of the subjects are males while one is female. All of the subjects are right-handed by self-report.

4.2. Apparatus

Two kinds of psychophysical experiments are conducted. One of them is the test of detection ability while the other is the test of discrimination ability. The experimental setup is shown in Fig. 7. The human subject manipulates the master device, which is a PHANToM Premium in this case. The virtual slave manipulator is interacting with a virtual wall as the environment. The teleoperation setup is implemented using Visual C++, and GUIs for detection test and discrimination test have been made to interact with the virtual environment as shown in Fig. 8a and b, respectively.

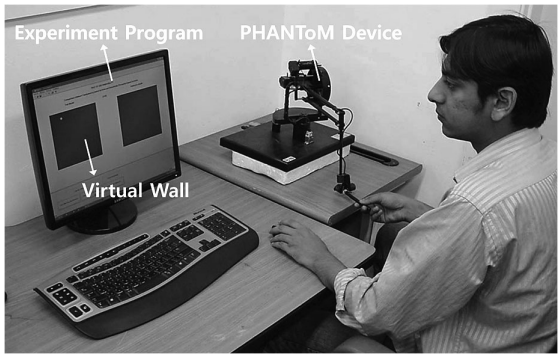

Figure 7. Experimental setup for psychophysics experiments.

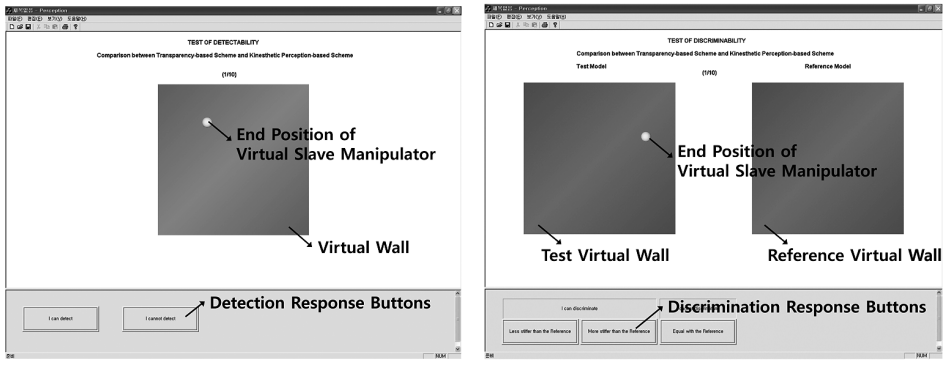

(a) (b)

Figure 8. Graphical user interface (GUI) for psychophysics experiments: (a) test of detection ability and (b) test of discrimination ability.

For the detection test, as shown in Fig. 8a, there is one virtual wall and the subjects are asked to respond as to whether they can detect the wall or not. The default color of the wall is red, but it turns blue as soon as the end-effector of the virtual slave manipulator touches the wall. The discrimination test, however, has two virtual walls. The subjects are asked to discriminate between these two walls based on the haptic information that is fed back to the subject. The haptic update rate was fixed at 1 kHz for the PHANToM haptic device. The experiments were designed according to within-subject design for cost efficiency and maintaining uniformity.

4.3. Procedure

Each subject has to perform the experiments for three different cases where each case is divided into two series, such as an ascending series and a descending series, which are generally defined by the method of limits [22]. The three cases differ according to the different lower limits for the ascending series and different upper limits for the descending series, and the variable step sizes that vary from case to case so as to rule out any possibility of intelligent guesses. Also, the cases and the series are all randomized so as to minimize the human response bias.

All the six trials (three cases $\times$ two series) are repeated for the kinesthetic perception-based control scheme and the transparency-based control scheme to obtain the comparison and verify the efficacy of the developed scheme. These are repeated for two kinds of force feedback system such as 100% force feedback and 80% force feedback of environment force. Therefore, each subject has to perform a total of 12 trials for the experiment to test the detection ability as well as another 12 trials for the experiment to test the discrimination ability.

4.4. Method

4.4.1. Test of Detection Ability

The test of detection ability is designed in such a way that a human subject who is holding the PHANToM is asked to interact with the virtual wall which is known as the test model and respond as to whether he or she can detect the impedance of the environment. Each subject has to perform the experiments for three different cases where each case is divided into two series, such as an ascending series and a descending series. The three cases differ according to the different lower limits for the ascending series and different upper limits for the descending series, and the variable step sizes that vary from case to case so as to rule out any possibility of intelligent guesses. Also, the cases and series are all randomized so as to minimize human response bias. The points at which the response changes from ‘cannot detect’ to ‘can detect’ for ascending series or *vice versa* for descending series are marked as transition points. The method of limits is used to calculate the AL for the subjects [25]. According to this method, at first, the average of the transition points for all the ascending series and the descending series are calculated. Then, the AL is calculated by taking the mean of the average transition points of both these series.

4.4.2. Test of Discrimination Ability

The GUI for the test of discrimination ability has two virtual walls — one of which is called the test model and the other reference model. Each subject is asked to respond if he or she can discriminate between the test model and the reference model. Every subject has to perform the experiments for three different cases in which the reference models have three different environment impedances. The reference model impedances are chosen uniformly such as $Z_e = 1 + 50/s$, $Z_e = 1 + 200/s$ and $Z_e = 1 + 500/s$. For each of these reference models there are two kinds of series known as an ascending series and a descending series, which is similar to that of the test of detection. For an ascending series, the initial impedance of the test model is much lower than that of the reference model. After the subject clicks his or her response, the test model impedance is increased while the reference model impedance is kept same and the response is given again. This process goes on until an upper limit is reached. At some point in this process, the human response changes from 'less stiff than reference model' to 'equal'. This point is marked as lower limen (L_l). After some more time, a point would come when the response changes from 'equal' to 'more stiff than reference model' and this point is marked as the upper limen (L_u). The series is stopped when an upper limit is reached.

For a descending series, the initial impedance of the test model is, however, much higher than that of the reference model. As the subject clicks his or her response, the test model impedance is decreased while the reference model impedance is kept the same. During the experimental procedure, the response changes from 'more stiff than reference model' to 'equal' and 'equal' to 'less stiff than reference model' at some points of time. These response transition points are termed L_u and L_l, respectively. The series is stopped when a lower limit is reached. The method of limits is also used to calculate the JND for the subjects [25]. According to this method, at first, the average of the upper limen and the lower limen for all the ascending series and the descending series of each reference model are calculated. Then, the DL is calculated by taking the difference of the mean of the upper limen and lower limen. The JND is calculated by taking the ratio of the DL and the reference stiffness.

4.5. Result

The experimental results of psychophysics experiments for test of detection ability and test of discrimination ability are summarized in Fig. 9 and Table 1 using AL and JND. JND is calculated using the experimental results of DL and the stiffness intensity of references, and it is expressed as a percentage in this work. Both the AL and the JND values are less for 100% force feedback as compared to 80% force feedback system except for the case of the JND when the stiffness intensity is 50 N/m, which is an irregular experimental outcome. However, on the whole, 100% force feedback gives better detection and discrimination due to lower AL and JND values. Therefore, it becomes more difficult to detect and to discriminate soft environments. This experimental result can be explained easily using the proposed kinesthetic perception region as shown in Fig. 10. The kinesthetic perception region

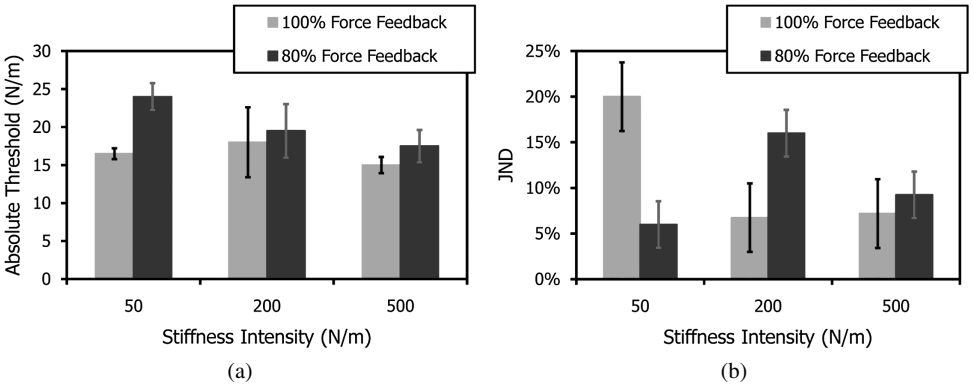

Figure 9. Experimental results: (a) AL and (b) JND.

Table 1.
Experimental results summary for test of detection ability and discrimination ability: AL and JND

	100% force feedback	80% force feedback
AL (N/m)	16.5	20.22
JND (%)	6.98	12.63

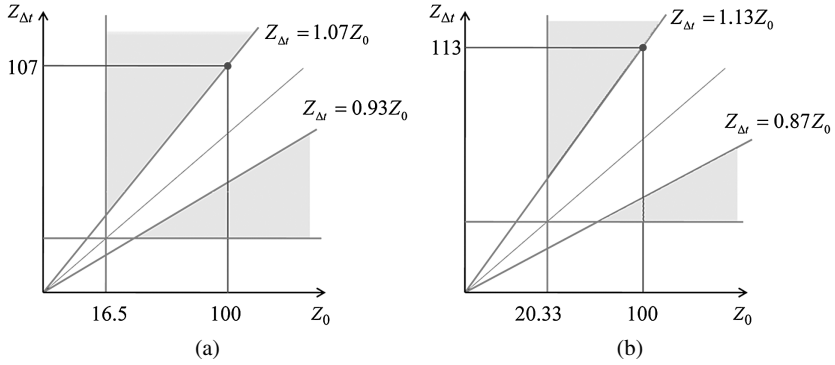

Figure 10. Kinesthetic perception region of psychophysical experiment results: (a) case of 100% force feedback and (b) case of 80% force feedback.

of the 80% force feedback system shown in Fig. 10b is smaller than that of the 100% force feedback system shown in Fig. 10a.

The kinesthetic perception region can be compared quantitatively using the proposed performance index for kinesthetic perception. If it is assumed that both $M_{\text{detection}}$ and $M_{\text{discrimination}}$ of the 100% force feedback system are 1, $M_{\text{detection}}$ and $M_{\text{discrimination}}$ of the 80% force feedback system are calculated as 0.81 and 0.55, respectively, using Table 1. Figure 11 shows the quantitative change of kines-

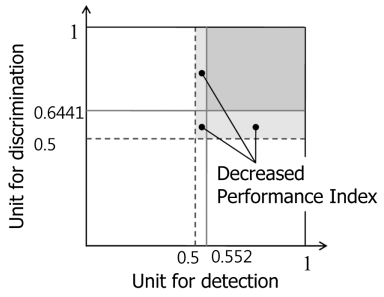

Figure 11. Change of the performance index for kinesthetic perception in psychophysical experiments.

Table 2.
Experimental results for test of detection ability and discrimination ability: AL and JND

	100% force feedback	80% force feedback
$M_{\text{detection}}$	1	0.81
$M_{\text{discrimination}}$	1	0.55
$PI_{\text{perception}}$	0.25	0.16

thetic perception performance based on Table 2. As a result, kinesthetic perception ability of the 80% force feedback is decreased by about 32.23% when compared to the 100% force feedback. Therefore, we can quantify and compare the kinesthetic perception ability of a certain force feedback system with that of the others using the proposed kinesthetic perception region and the performance index shown in Figs 4 and 5, respectively.

5. Experimental Results

5.1. Experimental Setup

5.1.1. A 1-d.o.f. Scaled Teleoperation System

An experimental setup, as shown in Fig. 12, was prepared using two 1-d.o.f. mechanical devices as the master haptic device and the slave manipulator.

A national Instruments motion controller was used together with a Maxon motor driving circuit to control the master and slave manipulator through a wire-driven mechanism. The control algorithm is implemented using MATLAB Simulink and Real-Time Windows Target Workshop is used to connect MATLAB Simulink with the control hardware. ATI six-axis force/torque sensors, Mini40 and Nano17, are attached to the master device and the slave manipulator, respectively, as shown in Fig. 13. A 16-bit A/D interface is used to input voltages from the force/torque sensors. The human operator perceives the environment by pushing the handle tip of the master device. The sampling time of the experimental system is 1 kHz.

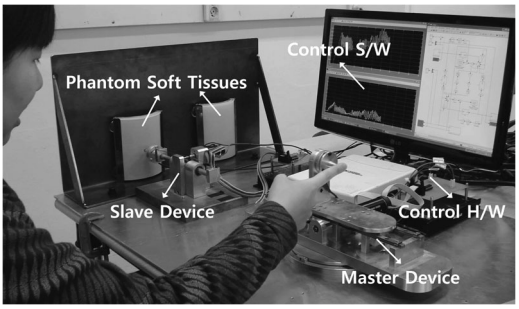

Figure 12. Experimental setup of the 1-d.o.f. scaled teleoperation system.

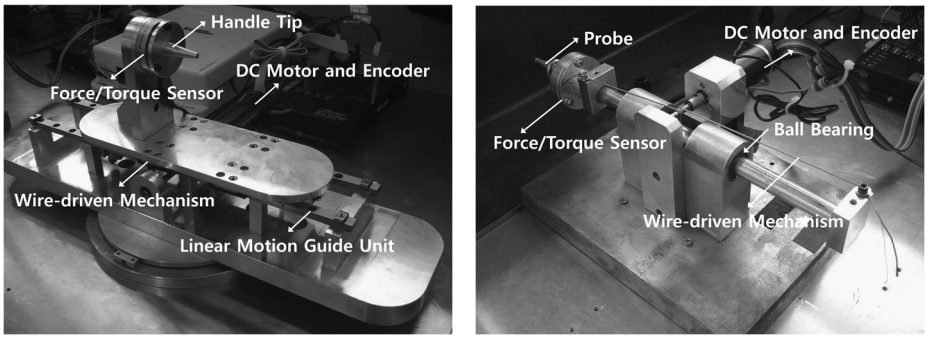

(a) (b)

Figure 13. Experimental devices: (a) master haptic device and (b) slave manipulator.

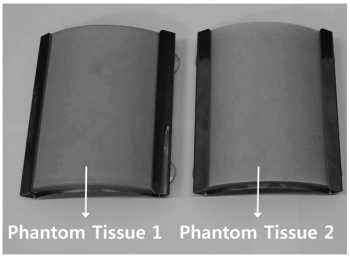

Figure 14. Phantom soft tissues.

5.1.2. Phantom Soft Tissues

Phantom tissues were used as the visco-elastic soft tissue environment as shown in Fig. 14. The characteristics of the phantom tissues are analyzed by measuring the interacting force and position. Figure 15 shows the stiffness characteristics of the phantom tissue. Although the stiffness of tissues is nonlinear, the stiffness of every phantom tissue is calculated under the assumption of linearity for small deflections. Results are $Z_{T1} = 522.31$ N/m and $Z_{T2} = 452.04$ N/m for the phantom tissue 1 and the phantom tissue 2, respectively.

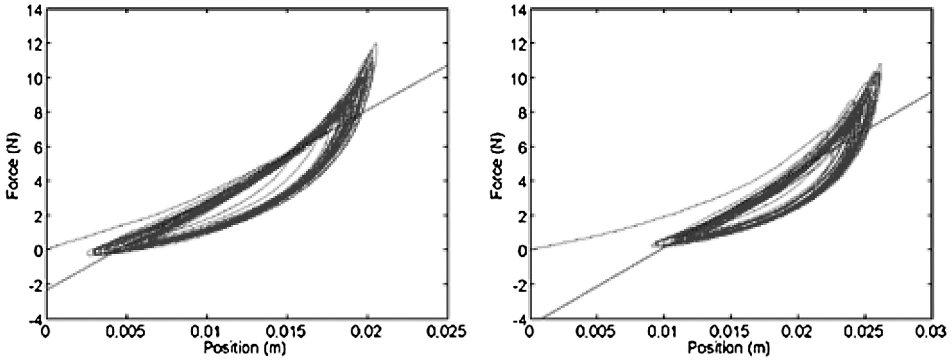

Figure 15. Stiffness characteristics of phantom soft tissues: (a) phantom tissue 1 and (b) phantom tissue 2.

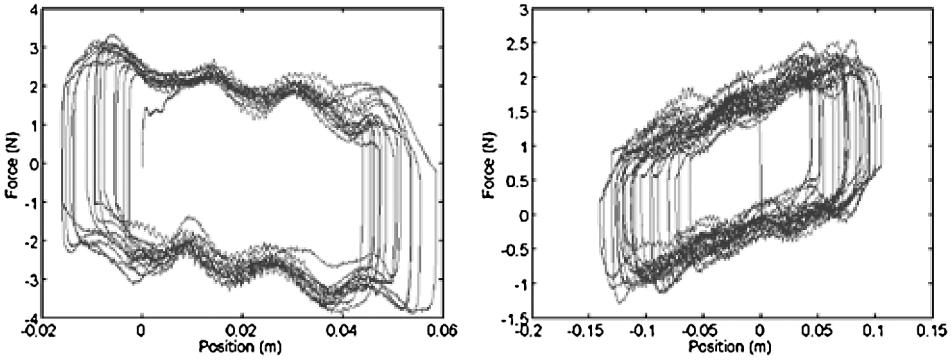

Figure 16. Force graph in free motion before friction compensation: (a) master haptic device and (b) slave manipulator.

5.1.3. Identification and Friction Compensation of Master and Slave Devices

Figure 16 shows the Coulomb friction of the master haptic device and the slave manipulator. Coulomb friction is compensated using estimated device parameters. The dynamics of the device is expressed as:

$$F_{\mathrm{h}}(t) = Ma(t) + Bv(t) + F_{\mathrm{c}}\,\mathrm{sgn}(v(t)), \tag{27}$$

where M, B and F_{c} are inertia, damping and Coulomb friction of the device, respectively, and these parameters are unknown. These unknown parameters are estimated using the measured input force of the human operator, $F_{\mathrm{h}}(t)$, and the position, $x(t)$. In this paper, the least-squares algorithm is used to estimate M, B and F_{c}. The master and slave device were randomly moved for 20 s by a finger, and this procedure was repeated 10 times. The estimation result is shown in Table 1. With these estimated parameters, feed-forward compensation of Coulomb friction is implemented; 95% of Coulomb friction is compensated using this feed-forward compensator as shown in Fig. 17 and Table 3.

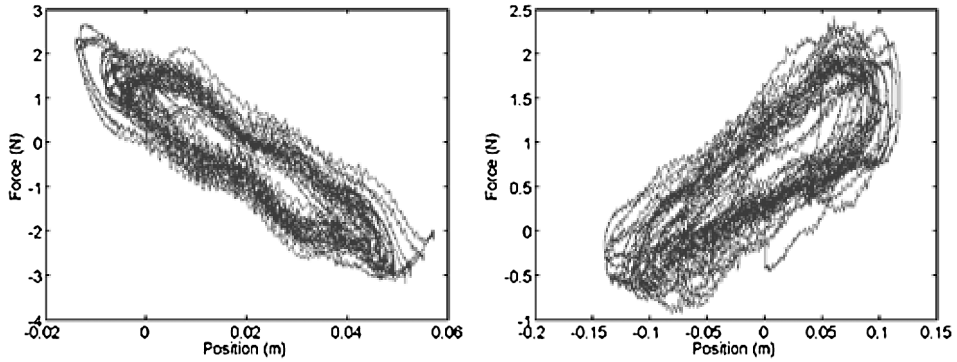

(a) (b)

Figure 17. Force graph in free motion after friction compensation: (a) master haptic device and (b) slave manipulator.

Table 3.
Device identification result

Device	Parameters	Without friction compensation	With friction compensation
Master	M (kg)	0.75	0.80
	B (Ns/m)	5.05	2.59
	F_c (N)	1.52	0.07
Slave	M (kg)	0.09	0.09
	B (Ns/m)	0.57	0.44
	F_c (N)	0.50	0.04

Finally, a local PD controller of the master and the slave is designed based on Ref. [27], and fine-tuned manually. The tuned controllers are $C_m = 33.72s + 722.52$ and $C_s = 3.6372s + 77.94$ for the master haptic device and the slave manipulator, respectively. All experiments were performed using the phantom tissues 1 and 2. All the experimental results are illustrated using the average values for the phantom tissues 1 and 2. The force and position scaling factors were chosen accordingly. We increased only the force scaling factor, S_f, because there is a limitation of workspace to increase the position scaling factor, S_p. In other words, we fixed the position scaling factor as 1 and increased the force scaling factor from 1 to several hundreds. This is valid because only the product of the position and force scaling factor affects the performance and stability.

5.2. Effect of Scaling Factors on Position Tracking

The experimental results show that the position tracking error decreases with the increase in the product of the scaling factors $S_p S_f$ as can be seen in Fig. 18. As we analyzed in Section 3, this trend is true for all control architectures. The PP control architecture shows the best position tracking as $S_p S_f$ is increased.

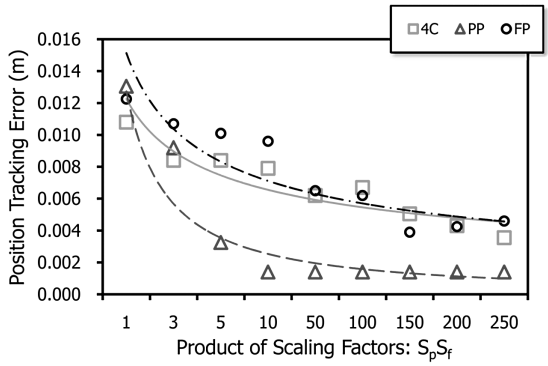

Figure 18. Experimental results for position tracking ability of the control architectures corresponding to the product of scaling factors.

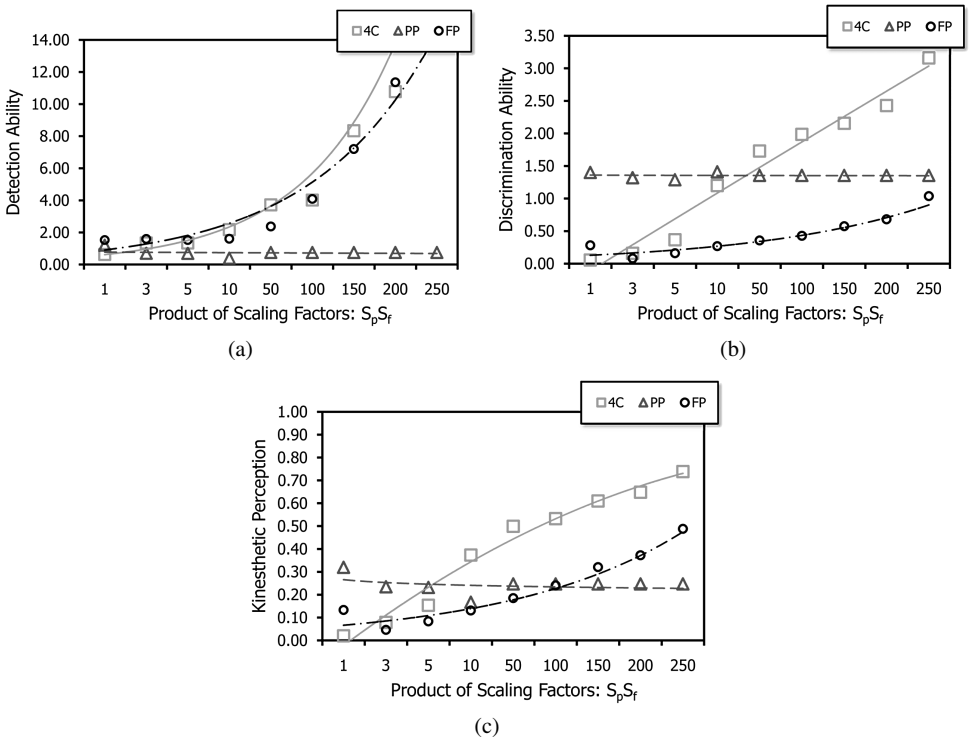

Figure 19. Experimental results for kinesthetic perception of the control architectures corresponding to the scaling factors: (a) detection ability, (b) discrimination ability and (c) kinesthetic perception.

5.3. Effect of Scaling Factors on Kinesthetic Perception

Figure 19 shows the experimental results for the detection ability and the discrimination ability. As with the analyzed results of the kinesthetic perception, the detection ability and discrimination ability also increase as S_pS_f increases for the

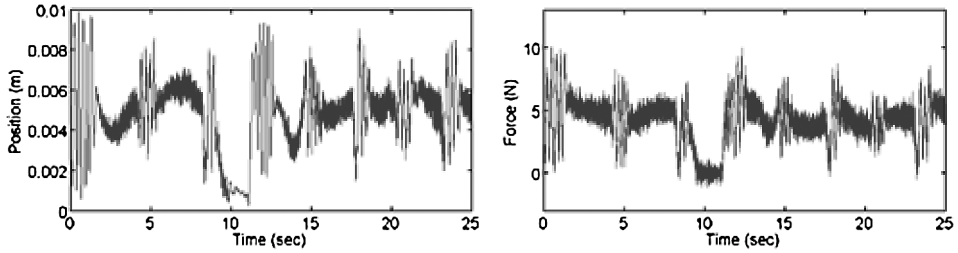

(a) (b)

Figure 20. Oscillation of the 4C control architecture with $S_p S_f = 350$: (a) position graph and (b) force graph.

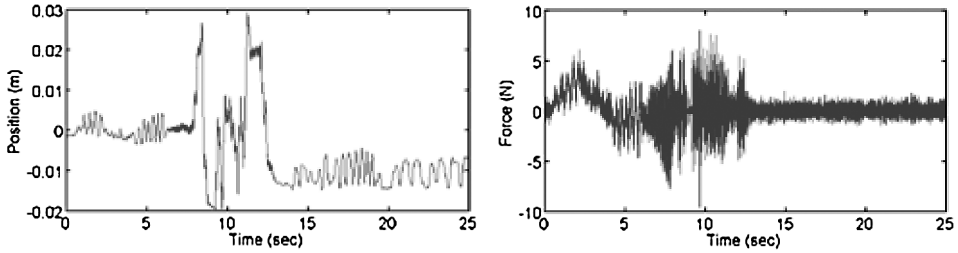

(a) (b)

Figure 21. Oscillation of the FP control architecture with $S_p S_f = 500$: (a) position graph and (b) force graph.

FP and 4C control architectures. However, unlike the previous mathematical analyses that show that the kinesthetic perception of the PP architecture is not affected by the scaling factors, the experimental results show a slight decrease of the kinesthetic perception in the PP control architecture with the increase in $S_p S_f$. However, this very slight decrease in the experimental results might be due to some uncertainties that might be present in the system and is negligible in practical applications.

5.4. Effect of Scaling Factors on Stability

It is apparent that the system becomes unstable with the increase in the product of the scaling factors $S_p S_f$ for the FP and 4C control architectures. In the case of the PP controller, $S_p S_f$ does not affect the system stability, similar to the analyzed result. Figures 20 and 21 show unstable phenomenon when $S_p S_f$ is 350 and 500 for the 4C and FP control architectures, respectively. It is, however, interesting to note that this unstable behavior is not divergent in nature, but is a continuous series of oscillations that are present in the system and can affect the system stability. A further increase in the scaling factors might lead to divergent instability.

6. Conclusions

The performance and the stability robustness of scaled teleoperation systems interacting with soft tissues have been analyzed in this study. First, position tracking

and kinesthetic perception are defined as parameters of the performance of the system. New performance indices are then proposed to evaluate the system performance quantitatively. In addition, a quantitative performance index for stability was proposed using Llewellyn's absolute stability criterion to evaluate the stability robustness and the stability bandwidth. The proposed performance index for kinesthetic perception is validated using psychophysical experiments.

The effects of scaling factors on the proposed performance indices for position tracking, kinesthetic perception and stability robustness are analyzed for PP, FP and 4C control architectures. The performance is enhanced and the stability robustness is decreased with the increase of the product of the scaling factors in the FP and 4C control architectures. In the case of PP control architecture, position tracking is not affected by the increase of the product of the scaling factors. There is also no effect of the scaling factors on the kinesthetic perception and stability robustness. The FP control architecture shows the best position tracking among the three kinds of controllers regardless of the scaling factors. The 4C controller shows the best kinesthetic perception. It is also shown that the stability robustness increases and the stability bandwidth decreases as the environment and the operator impedances become smaller.

Experiments are conducted using two kinds of phantom tissues that verify the existing tradeoff, and indicate that the performance of the position tracking and the kinesthetic perception increase while the stability decreases with the increase of the scaling factors. Results also show that the FP control architecture shows the best position tracking among the three kinds of controllers, regardless of the scaling factors, while the 4C controller shows the best kinesthetic perception. Therefore, based on the application-specific requirements, it is suggested to use the FP control architecture for maximum position tracking ability in applications that require the highest accuracy, but the 4C control architecture if the best kinesthetic perception is desired in applications that require minute detection and discrimination skills.

Based on the above results for analyses of performance, stability and scaling factors, our future work will focus on designing task-specific controllers for appropriate scaled applications and their requirements.

References

1. M. W. Noakes, L. J. Love and P. D. Lloyd, Telerobotic planning and control for DOE D&D operations, in: *Proc. Int. Conf. on Robotics and Automation*, Washington, DC, pp. 3485–3492 (2002).
2. T. B. Sheridan, Space teleoperation through time delay: review and prognosis, *IEEE Trans. Robotics Automat.* **9**, 592–606 (1993).
3. M. Utsumi, T. Hirabayashi and M. Yoshie, Development for teleoperation underwater grasping system in unclear environment, in: *Proc. Int. Symp. on Underwater Technology*, Tokyo, pp. 349–353 (2002).
4. H. Ming, Y. S. Huat, W. Lin and Z. H. Bin, On teleoperation of an arc welding robotic system, in: *Proc. Int. Conf. on Robotics and Automation*, Minneapolis, MN, pp. 1275–1280 (1996).

5. J. W. Hill and J. F. Jensen, Telepresence technology in medicine: principles and applications, *Proc. IEEE* **86**, 569–580 (1998).
6. J. E. Colgate, Robust impedance shaping telemanipulation, *IEEE Trans. Robotics Automat.* **9**, 374–384 (1993).
7. J. Yan and S. E. Salcudean, Teleoperation controller design using H_∞-optimization with application to motion-scaling, *IEEE Trans. Control Syst. Technol.* **4**, 244–258 (1996).
8. B. Hannaford, Kinesthetic feedback techniques in teleoperated systems, *Control Dyn. Syst.* **40**, 1–32 (1991).
9. S. E. Salcudean and J. Yan, Towards a force-reflecting motion-scale system for microsurgery, in: *Proc. Int. Conf. on Robotics and Automation*, San Diego, CA, pp. 2296–2301 (1994).
10. T. Sato, J. Ichikawa, M. Mitsuishi, H. Miyazaki and Y. Hatamura, Micro-teleoperation with manual task execution posture, *IEEE Control Syst. Mag.* **15**, 22–29 (1995).
11. C. R. Wagner, N. Stylopoulos, P. G. Jackson and R. D. Howe, The benefit of force feedback in surgery: examination of blunt dissection, *Presence Teleoperat. Virtual Environ.* **16**, 252–262 (2007).
12. M. C. Cavusoglu, A. Sherman and F. Tendick, Design of bilateral teleoperation controllers for haptic exploration and telemanipulation of soft environments, *IEEE Trans. Robotics Automat.* **18**, 641–647 (2002).
13. G. D. Gersem, H. V. Brussel and F. Tendick, Reliable and enhanced stiffness perception in soft-tissue telemanipulation, *Int. J. Robotics Res.* **24**, 805–822 (2005).
14. H. I. Son, T. Bhattacharjee and D. Y. Lee, Control design based on analytical stability criteria for optimized kinesthetic perception in scaled teleoperation, in: *Proc. ICCAS–SICE Int. Joint Conf.*, Fukuoka, pp. 3365–3370 (2009).
15. W. Iida and K. Ohnishi, Reproducibility and operationality in bilateral teleoperation, in: *Proc. IEEE Int. Workshop on Advanced Motion Control*, Kawasaki, pp. 217–222 (2004).
16. H. I. Son, T. Bhattacharjee, H. R. Jung and D. Y. Lee, Psychophysical evaluation of control scheme designed for optimal kinesthetic perception in scaled teleoperation, in: *Proc. IEEE Int. Conf. on Robotics and Automation*, Anchorage, AK, pp. 5346–5351 (2010).
17. P. Malysz and S. Sirouspour, Nonlinear and filtered force/position mappings in bilateral teleoperation with application to enhanced stiffness discrimination, *IEEE Trans. Robotics* **25**, 1134–1149 (2009).
18. S. S. Haykin, *Active Network Theory*. Addison-Wesley, Reading, MA (1970).
19. H. I. Son and D. Y. Lee, Two-channel control for scaled teleoperation, in: *Proc. Int. Conf. on Control, Automation and Systems*, Seoul, pp. 1284–1289 (2008).
20. B. Hannaford, A design framework for teleoperators with kinesthetic feedback, *IEEE Trans. Robotics Automat.* **5**, 426–434 (1989).
21. D. A. Lawrence, Stability and transparency in bilateral teleoperation, *IEEE Trans. Robotics Automat.* **9**, 624–637 (1993).
22. G. C. Burdea, *Force and Touch Feedback for Virtual Reality*. Wiley, New York (1996).
23. L. A. Jones, Kinesthetic sensing, in: *Proc. Workshop on Human and Machine Haptics*, Pacific Grove, CA, pp. 1–10 (1997).
24. B. Hannaford, Experimental measurements for specification of surgical mechanisms and understanding of surgical skill, in: *Lecture Notes of the European Summer School on Surgical Robotics*, Montpellier, pp. 805–822 (2003).
25. G. A. Gescheider, *Psychophysics: The Fundamentals*. Erlbaum, Mahwah, NJ (1997).
26. R. J. Adams and B. Hannaford, Stable haptic interaction with virtual environments, *IEEE Trans. Robotics Automat.* **15**, 465–474 (1999).

27. K. Hashtrudi-Zaad and S. E. Salcudean, Analysis of control architectures for teleoperation systems with impedance/admittance mater and slave manipulators, *Int. J. Robotics Res.* **20**, 419–445 (2001).
28. M. Minsky, O. Y. Ming, O. Steele, F. P. Brooks and M. Behensky, Feeling and seeing: issues in force display, *ACM SIGGRAPH Comp. Graphics* **28**, 235–270 (1990).
29. J. J. Gil, A. Avello, A. Rubio and J. Florez, Stability analysis of a 1 DOF haptic interface using the Routh–Hurwitz criterion, *IEEE Trans. Control Syst. Technol.* **12**, 583–588 (2004).

About the Authors

Hyoung Il Son received the BS and MS degrees from the Department of Mechanical Engineering, Pusan National University, South Korea, in 1998 and 2000, respectively, and the PhD degree from the Department of Mechanical Engineering, KAIST, South Korea, in 2010. He is currently a Research Scientist in the Department of Human Perception, Cognition and Action, Max Planck Institute for Biological Cybernetics (MPI), Germany. Before joining MPI, he was a Researcher in the Institute of Industrial Science, University of Tokyo, Japan, until March 2010. He also worked as a Senior Researcher in the Production Engineering Research Institute, LG Electronics, South Korea (2003–2005) and in the Mobile Display Center, Samsung Electronics, South Korea (2005–2009). His research interests include haptics, teleoperation and control of discrete event/hybrid systems.

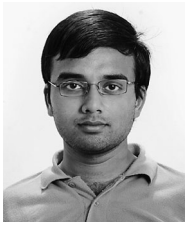

Tapomayukh Bhattacharjee received the BTech degree from the Department of Mechanical Engineering, National Institute of Technology, Calicut (NIT-Calicut), India, in 2006. He completed his MS degree at the Department of Mechanical Engineering, KAIST, South Korea, in 2009. He is currently working as a Visiting Scientist in the Cognitive Robotics Center, Korea Institute of Science and Technology (KIST), South Korea. He also worked as a Graduate Engineer Trainee in TAL Manufacturing Solutions Ltd, Tata Motors Campus, Pune, India (2006–2007). His research interests include haptics, teleoperation, manipulation and control of humanoid redundant arm systems, and humanoid hand–arm coordination.

Hideki Hashimoto received the BS, MS and DE degrees from the Department of Electrical Engineering, University of Tokyo, in 1981, 1984 and 1987, respectively. He joined the Institute of Industrial Science of the University of Tokyo as a Lecturer, from April 1987. Then, he has been an Associate Professor, from July 1990 to the present. He was a Visiting Scientist at LIDS (Laboratory for Information and Decision System) and LEES (Laboratory for Electromagnetic and Electronic Systems) of MIT from September 1989 to August 1990. He is an Invited Distinguished Professor at Seoul National University, from 2009 to 2011, and an Visiting Professor at Budapest University of Technology and Economics, from 2009 to 2011. He was an Administrating Committee Member of the IEEE IES and RAS, and Vice President of the IEEE IES and ITSC. He was the Founding General Chairman of the 1997 IEEE/ASME International Conference on Advanced Intelligent Mechatronics. He was a Program Chairman of IEEE/RSJ IROS 2000 and a General Chairman of IEEE ITS 2002. His research topics are intelligent systems, robotics and control. He is a Fellow of the IEEE.